International Journal of Applied Earth Observation and Geoinformation 42 (2015) 76–86

Contents lists available at ScienceDirect

International Journal of Applied Earth Observation and Geoinformation

journal homepage: www.elsevier.com/locate/jag

Open-pit mining geomorphic feature characterisation

Jianping Chen [a], Ke Li [a], Kuo-Jen Chang [b], Giulia Sofia [c], Paolo Tarolli [c,*]

[a] School of Earth Sciences and Resources, China University of Geosciences (Beijing), 100083 Beijing, China
[b] Department of Civil Engineering, National Taipei University of Technology, 10654 Taipei, Taiwan
[c] Department of Land, Environment, Agriculture and Forestry, University of Padova, Agripolis, viale dell'Università 16, 35020 Legnaro (PD), Italy

ARTICLE INFO

Article history:
Received 5 February 2015
Accepted 11 May 2015

Keywords:
Open-pit mine
UAV
SfM
DSM
SLLAC

ABSTRACT

Among the anthropogenic topographic signatures on Earth, open-pit mines are of great importance. Mining is of interest to geomorphologists and environmental researchers because of its implication in geomorphic hazards and processes. In addition, open-pit mines and quarries are considered the most dangerous industrial sector, with injuries and accidents occurring in numerous countries. Their fast, accurate and low-cost investigation, therefore, represents a challenge for the Earth science community. The purpose of this work is to characterise the open-pit mining features using high-resolution topography and a recently published landscape metric, the Slope Local Length of Auto-Correlation (SLLAC) (Sofia et al., 2014). As novel steps, aside from the correlation length, the terrace's orientation is also calculated, and a simple empirical model to derive the percentage of artificial surfaces is tested. The research focuses on two main case studies of iron mines, both located in the Beijing district (P.R. China). The main topographic information (Digital Surface Models, DSMs) was derived using an Unmanned Aerial Vehicle (UAV) and the Structure from Motion (SfM) photogrammetric technique. The results underline the effectiveness of the adopted methodologies and survey techniques in the characterisation of the main mine's geomorphic features. Thanks to the SLLAC, the terraced area given by open-cast/open-pit mining for iron extraction is automatically depicted, thus, allowing researchers to quickly estimate the surface covered by the open-pit. This information could be used as a starting point for future research (i) given the availability of multi-temporal surveys to track the changes in the extent of the mine; (ii) to relate the extent of the mines to the amount of processes in the area (e.g. pollution, erosion, etc.), and to (iii) combine the two points, and analyse the effects of the change related to changes in erosion. The analysis of the correlation length orientation also allows researchers to identify the terrace's orientation and to understand the shape of the open-pit area. The tectonic environment and history, or inheritance, of a given slope can determine if and how it fails, and the orientation of the topographic surface or excavation face, with respect to geologic features, is of major significance. Therefore, the proposed approach can provide a basis for a large-scale and low-cost topographic survey for sustainable environmental planning and, for example, for the mitigation of environmental anthropogenic impacts due to mining.

1. Introduction

Anthropogenic landscapes now cover a great deal of the Earth's surface (Ellis, 2004; Foley et al., 2005; Tarolli, 2014). In such landscapes, the direct anthropogenic disturbance of surface morphology and processes is significant (Ellis et al., 2006; Ellis, 2011; Vanacker et al., 2014). The progressive increase in intensive farming, industrialisation and urbanisation, aimed at servicing the needs of human populations, has transformed the natural landscapes by changing the topography, vegetation cover, physical and chemical properties of soil, and soil water balances (Tarolli et al., 2014). The analysis of human-landscape interactions in anthropogenic landscapes represents a challenge for better understanding the evolution of our present-day environment. This analysis can contribute to steering integrated environmental planning towards sustainable development, and can mitigate the consequences of anthropogenic alteration (Tarolli et al., 2015). Among the most evident landscape signatures of the human fingerprint (e.g. road networks and agricultural practices such as terracing), open-pit mines are of great importance. Mining is an activity integral to modern society that has a long history and occurs in a wide range of geomorphic settings. Mining activities can have a significant impact on the geomorphology and hydrology of catchments, both dur-

* Corresponding author. Tel.: +39 49 8272677; fax: +39 49 8272686.
E-mail address: paolo.tarolli@unipd.it (P. Tarolli).

http://dx.doi.org/10.1016/j.jag.2015.05.001
0303-2434/

Fig. 1. Daye iron mine, Hubei Province (P.R. China); one of the largest open-pit mines in Asia (Photo by Alex Chi – Panoramio®).

ing mining and for many years post-mining (Hancock et al., 2008; Herrera et al., 2010). According to Wilkinson (2005), humans move increasingly large amounts of rock and sediment during various construction activities, thus, becoming a geological agent. Mining has also become of interest to geomorphologists and environmental researchers because of its implications for geomorphic hazards and processes (Mossa and James, 2013). Open-pit mining imposes severe ecological effects on the land, with alterations that affect vegetation, soil, bedrock and landforms (Martín-Duque et al., 2010), which contribute to changes in surface hydrology, groundwater levels and flow paths (Osterkamp and Joseph, 2000; Nicolau and Asensio, 2000). In addition, open-pit mines and quarries are considered the most dangerous industrial sector, with injuries and accidents occurring in numerous countries such as the United Kingdom (e.g. Foster et al., 2008), South Africa (e.g. Hermanus, 2007), the USA (e.g. Esterhuizen and Gürtunca, 2006) and China (Zhangtao, 2010). A recent statistical study ranked Chinese coalmines among the top three sources of fatalities in the country (Zhangtao, 2010). Data for other developing countries are not available, but the media provides some indication of the current status of the global mining industry, painting a rather similar picture (Badri et al., 2011).

The assessment of open-pit mines as case studies is important, considering that (1) mining significantly affects the Earth's surface and its related processes (e.g. erosion); (2) the increase in raw-material demand connected to an increase in the population (the global production of concrete, steel, aluminium, copper and glass will significantly increase by 2050 (Vidal et al., 2013); and (3) only a few analyses are available in the Earth Science community discussing and quantifying the role of open-pit mines as one of the major anthropogenic forcing (i.e. Osterkamp and Joseph, 2000; Nicolau and Asensio, 2000; Rigina, 2002; Martín-Duque et al., 2010). Fig. 1 shows an example of an iron open-pit mine in China, where the characteristic terraces that affect the landscape are clearly visible, creating a significant topographic signature.

Analysing open-pit mines through geomorphology, therefore, can provide a useful framework both for an understanding of their environmental effects, including changes in erosion-sedimentation processes and soil properties (Wilkinson and McElroy, 2007), and the design of the most appropriate strategies for reclamation (Toy and Hadley, 1987). In the last decade, a range of new remote-sensing techniques has led to a dramatic increase in terrain information, providing new opportunities for a better understanding of Earth surface processes based on geomorphic signatures (Tarolli, 2014). Light detection and ranging (LiDAR) technology (Slatton et al., 2007; Roering et al., 2013) and, more recently, Structure from Motion (SfM) photogrammetry (Westoby et al., 2012; Fonstad et al., 2013; Javernick et al., 2014; Micheletti et al., 2014; Prosdocimi et al., 2015) provide high resolution topographic data with notable advantages over traditional survey techniques. A valuable characteristic of these technologies is their capability to produce sub-meter resolution digital terrain models (DTMs), and high-quality land coverage information (digital surface models, DSMs) over large areas (Tarolli et al., 2009; Pirotti et al., 2012; Passalacqua et al., 2014). LiDAR high-resolution topographic surveying is traditionally associated with high capital and logistical costs, so that data acquisition is often passed on to specialist third party organisations (Westoby et al., 2012). UAVs (unmanned aerial vehicles) on the other hand, offer a remote sensing tool capable of acquiring high-resolution spatial data at an unprecedented spatial and temporal resolution at an affordable cost (Westoby et al., 2012). The scientific community is now providing a significantly increasing amount of analyses on the Earth's surface using UAVs in different environmental contexts (Jaakkola et al., 2010; Watts et al., 2012; Colomina and Molina, 2014; Hugenholtz et al., 2013; Woodget et al., 2015; d'Oleire-Oltmanns et al., 2012; Mancini et al., 2013; James and Robson, 2014; Lucieer et al., 2014; Mesas-Carrascosa, 2014).

Although high-resolution data and UAV technology have been increasingly used in the last few years, there are only a few published references related to their applicability in open-pit mining (e.g. Francioni et al., 2015). Currently, geologists and mining engineers use simplified representations of slope geometry to assess mineral resources, mining reserves, and final pit layouts (Grenon and Laflamme, 2011). At the same time, mining slope monitoring is generally done using radar, geodetic prisms, visual observations and other geotechnical instruments (Severin et al., 2014). Comparatively fewer studies have comprehensively examined the use of remote sensing to map surface mine extent, especially through time (e.g. Townsend et al., 2008). Therefore, the main goal of this paper is to establish (and test) a rapid, low-cost methodology to characterise the open-pit mining geomorphic features using UAVs and digital terrain analysis based on SfM elevation data. A local scale rapid geomorphologic characterisation of mines could be used to support sustainable environmental planning and mitigate the consequences of anthropogenic alterations due to mining.

2. Study area

The Miyun Iron Mine (Fig. 2a), located at Juge Town (117°1′54″E, 40°22′51″N) in the northeast suburb of Beijing and on the south end of the Miyun Reservoir, is one of the largest mines in Beijing. The mine covers an area of 17 km^2, making it one of the biggest state-owned enterprises in Beijing, reserving more than 140 million tonnes of iron ore. It was founded in 1959 and became operational in 1970. As of today, the main product of the company is iron powder. In its early stage of construction, the mine was designed as a multiple open-pit mine with potential for underground development as well. For more than 40 years, this mine hardly modified the morphology of the area; a hill with an altitude of 240 m was turned into a giant pit with a diameter of about 700 m and a bottom altitude of about −40 m. The field sites considered in this study consist of two opencast mines (mine I and mine II in Fig. 2b–c, respectively) as part of the large Miyun Iron Mine area. The mine areas include active extraction sites (about 1.6 km^2 in mine I and 1.5 km^2 in mine II), administrative areas and small villages.

2.1. UAV data specifications

A UAV survey was carried out during the summer of 2014. The aircraft used was a Skywalker X5 (Fig. 3). This is a small, fixed wing UAV, measuring 0.6 m in length, with a 1.2 m wing span. It

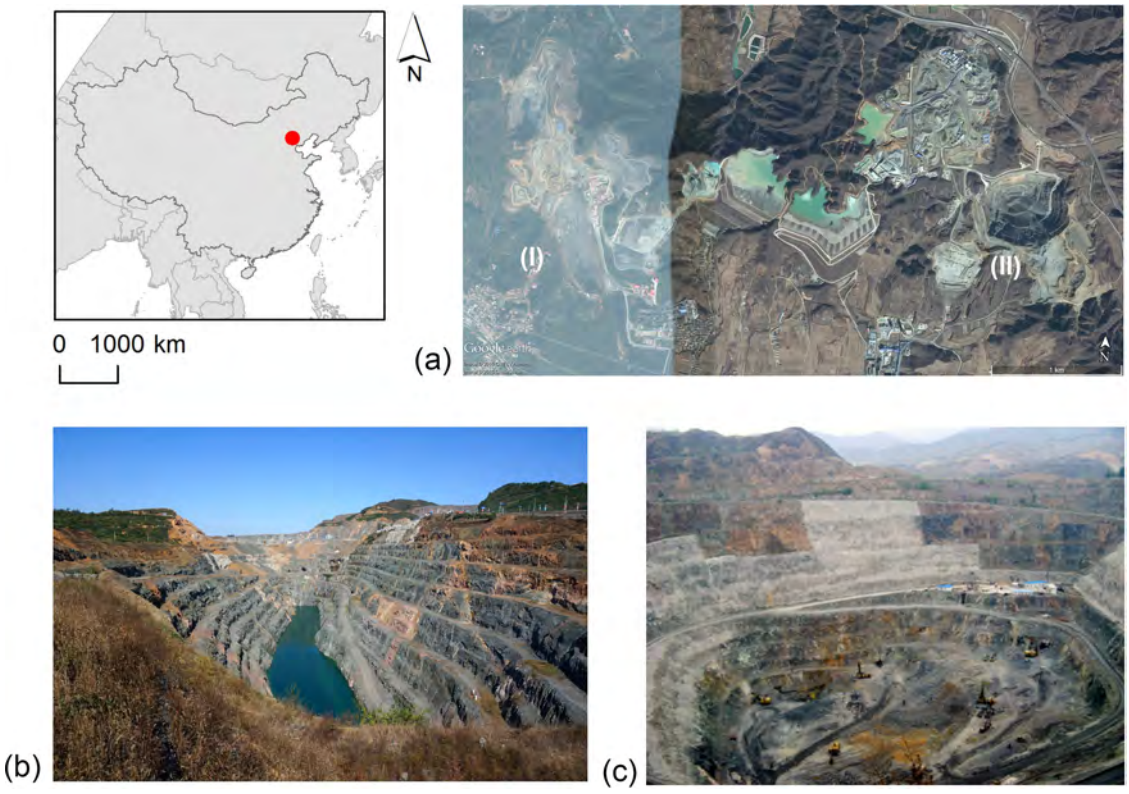

Fig. 2. Location map of the Miyun Iron Mine (a) and pictures of the two analysed iron open-pit mines (Beijing District, P.R. China): mine I (b) and mine II (c).

weighs less than 2.5 kg and can fly for up to 40 min using four-cell 3500 mah Li-Ion polymer batteries. The UAV, thanks to the autopilot, can autonomously fly along pre-defined flight paths and take photos at certain intervals, while also radio-communicating with a ground control system (GCS). From the UAV, colour photos were acquired using a Sony QX100 camera (20.9 M pixel resolution) (Fig. 3) equipped with a Carl Zeiss 10.4–37.1 mm lens and 1.0″ Exmor R CMOS sensor. Tables 1 and 2 show the flight characteris-

Fig. 3. 3D-view of the point cloud with coupled RGB colours for the surveyed mines I (a) and II (b). In In addition, notice a detail regarding the UAV used for the survey over the iron mining area and the mounted Sony Cyber-shot DSC-QX100 camera for the photograph collection.

Table 1
UAV flight plan over the two study areas.

	Flight No.	Flight height (relative)	Flight orientation	Flight lines	Photo interval (m)	Stripes interval (m)	Overlap single stripe (%)	Overlap between stripes (%)
Mine I	Flight A	250 m	N-S	8	40	190	81.04%	40.06%
Mine II	Flight B	200 m	N-S	12	40	95	76.33%	62.45%
	Flight C	250 m	E-W	9	40	150	81.04%	52.37%

Table 2
UAV flight specifications for the two study areas.

	Flight No.	Photo count	Flight length (m)	Flight time (min)	Average speed (m/s)	GCPs
Mine I	Flight A	499	20831	17	20	13
Mine II	Flight B	488	20172	17	20	10
	Flight C	516	21532	17.5	20	10

tics for both mines I and II; limited by the regulation and endurance of the UAV, the survey was planned separately for the two sites.

Prior to image acquisition and survey, we calibrated the camera and set high-accuracy ground control points (GCPs) (13 for Mine I, and 10 for Mine II) using painted markings of 0.2 × 0.2 m width. For better visibility, the GCPs were placed near artificial features and measured using D-GPS before the survey.

2.2. Digital surface model

The SfM technique was applied to obtain a 3D georeferenced point cloud from which a digital surface model (DSM) was derived. The data were processed using the Agisoft PhotoScan® photogrammetric software package (v1.0.4, build1847, http://www.agisoft.com/). The considered workflow comprised of the following main steps: (i) image import, (ii) image alignment, (iii) georeferencing, (iv) optimisation of image alignment and (v) creation of the point cloud. After the alignment, all photos were oriented, and the raw point cloud was georeferenced. Based on the estimated camera positions, PhotoScan® calculates depth information for each camera to be combined into a single dense point cloud dataset. The GCPs are then used to optimise the camera positions and the orientation of the data, which allow for better accuracy and reconstruction results. Table 3 reports the georeferentiation errors calculated by PhotoScan® along x, y and z axes for each 3D point cloud obtained by the SfM methodology.

After producing the point cloud, points were further manipulated using the open source programme CloudCompare® (http://www.danielgm.net/cc/). The points were further filtered to remove additional noise that typically affects these data, as also underlined by Javernick et al. (2014). In this case, the noise removal was accomplished manually: outlier values were, in fact, clearly visible as points completely outside the range of elevation values of the mine sites.

Fig. 3 shows the 3D view of the SfM point cloud for the two investigated mines coupled with RGB colours. The elevation points were then interpolated using the natural neighbour method (Sibson, 1981), which has already been proven useful for geomorphic analysis (Pirotti and Tarolli, 2010; Lin et al., 2013; Tseng et al., 2015), to generate 1 m resolution DSM. The vertical accuracy (RMSE – root mean square error – of elevation), evaluated by a direct comparison with ground differential GPS (DGPS) elevation points, was estimated in flat areas to be about 0.1 m, which is in line with previous works on UAV and SfM.

Table 3
Georeferentiation errors (Root Mean Square Error -RMSE) calculated by PhotoScan® along x, y and z-axes for each 3D point cloud obtained by the SfM methodology.

	x (m)	y (m)	z (m)
Mine I	0.14	0.15	0.16
Mine II	0.14	0.15	0.13

3. Methodology

3.1. Slope local length of auto-correlation

The characterisation of the open-pit mines is based on the morphological indicator proposed by Sofia et al. (2014): the Slope Local Length of Auto-Correlation (SLLAC), which quantifies the local self-similarities of slopes. The SLLAC is mainly intended to identify elongated elements without considering their steepness, but rather the variability and similarity of their slope. This work starts from a DSM, where elements, such as vegetation and buildings, are depicted; these elements might result in slope peaks on the map. Therefore, the use of a parameter that does not consider slope steepness is appropriate. After computing the slope as a derivative of the biquadratic function proposed by Evans (1980), the SLLAC is obtained using a moving window (kernel) approach. The procedure consists of two steps (Fig. 4): (1) the correlation γ (Fig. 4b) is computed between a slope square template (T in Fig. 4a) and its neighbouring area (W in Fig. 4a); (2) once the correlation map is derived, it is possible to compute the characteristic length of correlation (Fig. 4c).

The cross-correlation (Fig. 4b) is computed according to the formula described in Haralick and Shapiro (1992) and Lewis (1995):

$$\gamma_{(i,j)} = \frac{\sum_{u,v}(W_{(i+u,j+v)} - \overline{W}_{i,j})(T_{u,v} - \overline{T})}{\left(\sum_{u,v}(W_{(i+u,j+v)} - \overline{W}_{i,j})^2 \sum_{u,v}(T_{u,v} - \overline{T})^2\right)^{0.5}} \quad (1)$$

assuming a neighbouring area W of a size $M \times M$, and a square slope template T of size $N \times N$ (Fig. 4), indices (i,j) are row and column position of each pixel within W and they are valid in $1 \le i \le (M - N)$ and $1 \le j \le (M - N)$, while indices (u,v) run across $1 \le u \le N$ and $1 \le v \le N$. $\overline{W}$ is the local mean slope of the neighbourhood W underneath the slope template T whose top left corner lies on pixel (i,j). $\overline{T}$ is the mean value of the slope patch.

By choosing a threshold of the cross-correlation map (Fig. 4b) corresponding to the 37% of its maximum value (ISO 25178-2, 2013), we can derive the correlation length (Fig. 4c), which is, by definition, the length of the longest line passing through the central pixel and connecting two boundary pixels in the extracted area, which includes the central pixel (Fig. 4c).

In general, the size of the template (T) should be wide enough to capture at least the change in slope between the terrace wall and the terrace bench. Sofia et al. (2014) tested a fixed size of the template (10 m × 10 m) and the moving window W (100 m × 100 m), both on real and simulated DTMs having different terrace sizes, proving, therefore, the robustness of the chosen measures, inde-

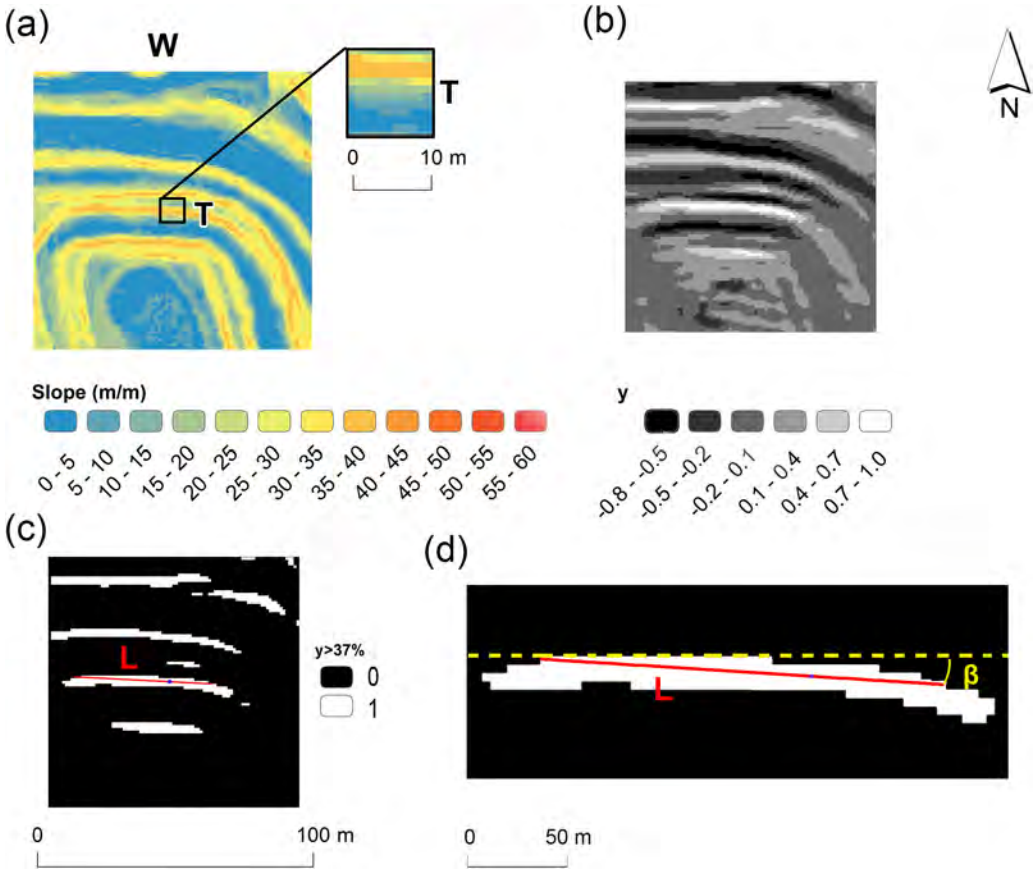

Fig. 4. Example of the calculation of SLLAC for a single moving window (W). (a) For each moving window (W), a slope template T is identified, having the centre at the centre of W. The cross-correlation between T and W is computed (b). The resulting map is thresholded at 37% of its maximum value (c). The length of correlation is then the length of the longest line passing through the central pixel (blue dot) and connecting two boundary pixels in the extracted area connected to the central pixel. (d) Measurement of the length orientation β(in this example, it is about −10°).

pendent of the terrace size and shape. The same work showed that increasing the size of the template and the kernel results in an increase in the computational time; thus, changes in sizes are not recommended. As a general approach, therefore, we applied the kernels identified in Sofia et al. (2014) (100 m × 100 m for the main moving window, and 10 m × 10 m for the slope template), as they were proven applicable to various mountainous contexts and terracing systems.

The SLLAC map can be further analysed using the Spc parameter (Surface Peak Curvature), which allows users to uniquely characterise a surface (Stout et al., 1994). The Spc is defined as for every peak:

$$\mathrm{Spc} = -\frac{1}{2n}\Sigma_{i=1}^{n}\left(\frac{\partial^2 z(x,y)}{\partial^2 x}\right) + \left(\frac{\partial^2 z(x,y)}{\partial^2 y}\right) \quad (2)$$

In the equation, a peak is defined as a pixel where all eight neighbouring pixels are lower in value, n is the number of considered peaks, z corresponds to the analysed map value (in this case, the SLLAC value), and x and y represent cell spacing (Stout et al., 1994).

3.2. Research novelties

After computing the correlation length (Section 3.1), we approached the computation of the orientation of such length (Fig. 4c). Determination of terrace orientation is, in fact, useful to better integrate the work of the geomechanical group into the terrace's creation process (Grenon and Laflamme, 2011). Focusing on the region in the analysis, the orientation is the angle (in degrees, ranging from −90° to 90°) between the longest line passing through the central pixel and connecting two boundary pixels and the x-axis (Fig. 4c). Knowing the orientation of the x-axis (in respect to North), and that the fibres in the SLLAC follow the orientation of the anthropogenic structures, their orientation can be a proxy for the orientation of the terrace's walls with respect to the cardinal directions, thus, providing a tool to analyse the shape of the mines and the organisation of the terraces.

As a further innovation, in this work, we propose a simple empirical model able to derive the percentage of an artificial surface given the Spc (Eq. (2)) value. According to Sofia et al. (2014), in fact, the higher the Spc, the lower the area within the study site covered by terraces. In the mentioned paper, the authors provided a simple example of this relationship using only two simulated DTMs. When working with a DSM, vegetation and buildings can be present in the model; thus, it is important to account for a higher variation of elevations, which can result in elevation isolated values whose conformation could influence the SLLAC, determining a high Spc also when terraces are present. Using a Monte Carlo simulation by considering multiple random realisations of a DTM, it is possible to account for the presence of different elements on the surface. In a Monte Carlo simulation, each map is recognised as only one possible realisation of the elevation surface, and multiple simulations can be used to quantify uncertainty through the evaluation of statistics associated with a distribution of realisations (e.g. Lanter and Veregin, 1992; Openshaw et al., 1991; Heuvelink et al., 1989; Sofia et al., 2013). Having multiple SLLAC maps and derived values of the Spc allows researchers to create a robust model that describes the variation of this index as a function of the terrace coverage using

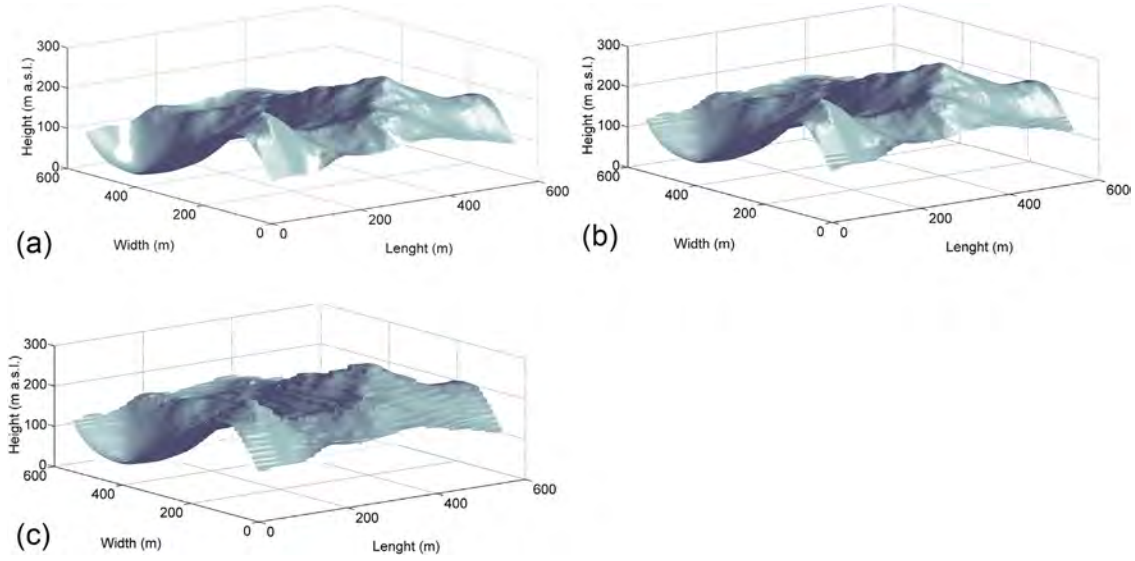

Fig. 5. (a) An example of a synthetic DTM. The same DTM having terraces covering (b) 50% and (c) 100% of the area.

a mean Spc value from all the simulated DTMs for each percentage of coverage. This can be considered a good estimate of the 'true' value of Spc caused by each specific coverage. Furthermore, the full range of values allows for the definition of confidence bounds for this relationship, identifying its limit and validity.

Given the results of Sofia et al. (2014), where 10 DTMs were simulated to analyse the variation of the Spc at the increasing of the terraced area, we decided to replicate the procedure creating 100 random maps of natural landscapes; thereafter, we added terraces covering pre-defined areas (0–100%). We simulated the synthetic DTMs using the same stochastic 2D multi-fractal random field (Schertzer and Lovejoy, 1989) using the same parameters considered by the original SLLAC work for the Mediterranean areas. The morphology of the study sites considered in this work is, overall, smooth, and the terraces of mining activities are similar to the agricultural Mediterranean terraces, following the mine contour lines, and having narrow and flat benches, and nearly vertical risers. The presence of outlier elevation values (buildings, vegetation, etc.) can be accounted for by considering the multiple random realisations of the surface. See Schertzer et al. (2013) for a more detailed description of the algorithm and the ranges of values that each coefficient can assume. The coefficient values were chosen arbitrarily, without any physical interpretation: their purpose is simply to create a realistic dataset in terms of height ranges and morphology (Fig. 5a).

Once the 100 DTMs were created, we manually added terraces using a posterization-like approach (Sofia et al., 2014). At first, we divided each map into 10 set intervals (covering 0–100% of the area, Fig. 5b and c). Then, we progressively layered each interval into steps, creating several regions of fewer values with abrupt changes from one to the other. The abrupt changes were created by collapsing all values in each region to their lower bound values.

Once all the maps were created, we computed the SLLAC and the derived Spc and plotted the Spc values against the increasing of the terraced areas. For further analysis, and to reduce the effects of minor observation errors, we considered the Spc values binned in 10^{-2} m^{-1} intervals plotted versus the average percentage coverage for each bin. For these binned average values, we created a model representing the increasing of the percentage at the decreasing of the Spc considering a polynomial approach. The main advantage of polynomial fits is that the data are reasonably flexible. In addition, the data are not too complicated, and they are linear, which means the fitting process is simple and can be easily implemented. The data are robust to noise and measurement errors (Abo Akel et al., 2007), and are not affected by truncation errors, round-off errors or unstable systems (Ralston and Rabinowitz, 1978).

After different trials, we found that the most adequate values were given by a third-degree polynomial in the form of:

$$\mathrm{Perc}_{\mathrm{art}} = p_1\mathrm{Spc}^3 + p_2\mathrm{Spc}^2 + p_3\mathrm{Spc} + p_4 \quad (2)$$

where $\mathrm{Perc}_{\mathrm{art}}$ is the percentage of an artificial surface within the study site, Spc is the second derivative of peaks (Eq. (2)) and p_1 to p_4 are empirical coefficients. However, when increasing the degree of the polynomial results in similar fits, however, high-degree fits can become unstable; therefore, we selected the third degree as optimal.

Fig. 6 shows the Spc for the simulated DTMs, the binned average values, the derived curve fitting, the Spc for the Mediterranean dataset (Sofia et al., 2014) and the confidence interval, while Table 4 shows the values of the polynomial coefficients.

To test the extent to which the Spc could identify anthropogenic landscapes, we compared values using a Mann–Whitney test. We deemed the Spc values obtained for the artificial landscapes areas having more than 10% of a terraced surface, following Sofia et al. (2014) as the basic populations, and we tested these values against the values that we derived from our study areas.

4. Results and discussion

Fig. 7 shows the obtained SLLAC map for the two mines (a, b). As expected, the SLLAC presents elongated elements (defined as fibres in Sofia et al., 2014) that follow the mine terraces. These fibres are mainly located within the extraction sites (open-pits and yellow boundaries in Fig. 7), they are circular and well-organised, and they follow the terrace walls. The two maps have a Spc of $3.8{\cdot}10^{-2}$ and $3.9{\cdot}10^{-2}$ m^{-1}, respectively. By comparison with the Spc of the simulated DTMs having more than 10% terraced areas the same threshold proven to be statistically significant in Sofia et al. (2014), the obtained p-value is about 0.2 in both cases, demonstrating that the obtained Spc is statistically similar to the ones of the artificial

Table 4
Parameters of the polynomial fittings obtained for the simulated landscape. The coefficients p_1–p_4 refer to Eq. (2).

p_1	p_2	p_3	p_4	R^2
2.402e+07	−2.892e+06	1.087e+05	−1209	0.87

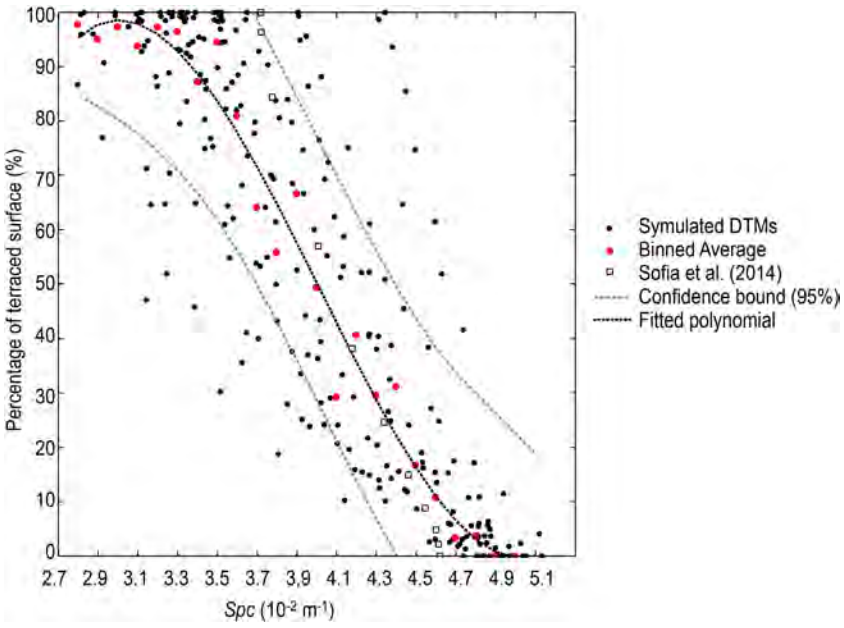

Fig. 6. Spc for the simulated DTMs, the binned average values and the derived curve fitting, as compared to the Spc for the Mediterranean dataset (Sofia et al., 2014). The 95% confidence interval is also showen.

landscapes. By applying the polynomial function (Eq. (3)), we estimated a terraced surface of about 63% and 49% for the two sites, respectively. If we consider the extent of mine I and mine II, we can estimate a mine terraced area of about 2.1 km^2 and 1.6 km^2, respectively. By measuring the mine area covered within the SLLAC extent (the yellow boundaries in Fig. 7) from the aerial photo, we can estimate a total terraced area of about 1.6 km^2 (mine I) and 1.5 km^2 (mine II). When considering mine II, the mine extent automatically identified from the SLLAC, is a suitable approximation of the actual extent of the mines. When considering mine I, however, there is a slight approximation of the values. This is because, in the south-eastern part of the mine (see Fig. 3a), there are buildings belonging to the mine company and long roads captured by the DSM: these elements contribute to creating fibres on the SLLAC. To this point, one could expect long isolated roads to have a longer correlation length and a different organisation in the landscape than that of a terrace. At the same time, short roads and areas with buildings would likely have a different organisation in the landscape, which could be captured considering the orientation of the correlation length (more random orientations within smaller areas). However, if we include the area in the open-pit mine, from the aerial photo, we can measure a total anthropogenic surface of about 2 km^2, which is in line with the one estimated from the polynomial approach.

By analysing, in detail, the SLLAC maps, we can observe that, generally, areas within the open-pit seem to have higher correlation lengths with respect to areas outside the mine open-pit. Fig. 8 shows the boxplots of SLLAC for areas within the pit and areas outside the pit.

In both mines, it appears that areas within the extraction sites show a higher mean SLLAC (median is 43.4 m for mine I and 35.1 m for mine II) when compared to the surrounding areas (median of 9.2 m and 11.7 m for mine I and mine II, respectively). In addition, areas within the pits show a higher variability (higher interquartile

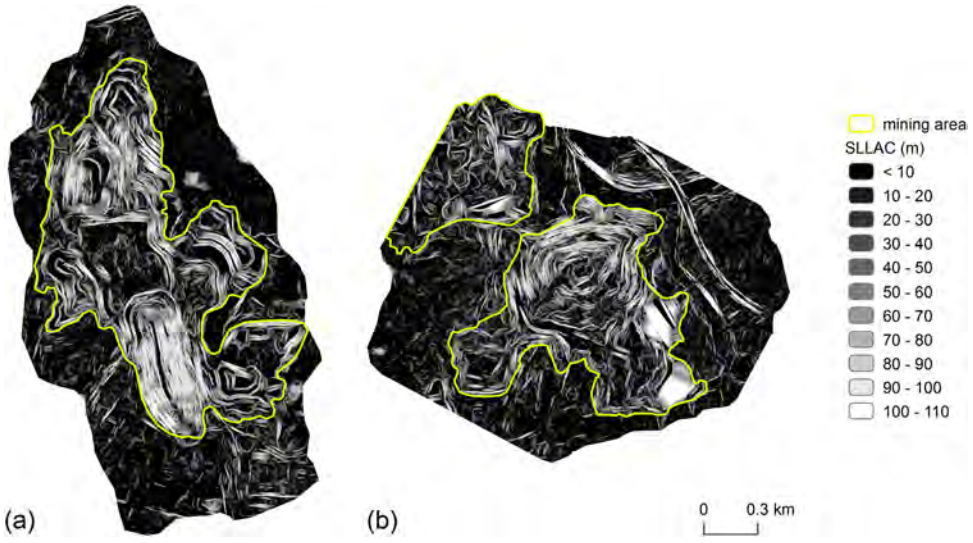

Fig. 7. SLLAC maps for mining sites I and II (a and b). The yellow boundaries represent the extent of the extraction areas within the mine sites.

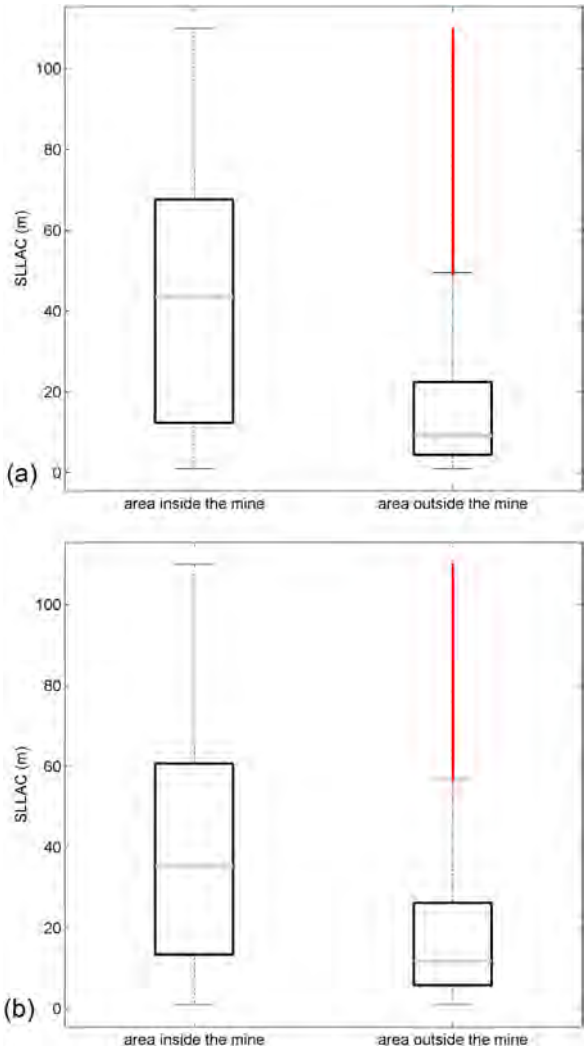

Fig. 8. A boxplot of the SLLAC values considering the extraction areas (highlighted in yellow in Fig. 7) as compared to the surroundings. (a) and (b) in the figure correspond to mining site I and II.

range, as represented by the boxes in the boxplots). This is because terraces have different physical lengths, lengths, which implies a different correlation length as well. Areas outside the pits are covered with vegetation and present buildings, and these elements are point-type elements or, generally, they present short and scattered shapes: this results in short and irregular fibres, having similar short correlation lengths. Even if areas outside the pit show fibres with high SLLAC values, they are generally isolated elements that represent outliers in the SLLAC distribution, and are mainly related to the presence of roads. As previously discussed (Fig. 8), it appears that SLLAC values related to terraces are generally high; it appears the terraces correspond to SLLAC values greater than at least one standard deviation of SLLAC. Numerous studies in the literature underlined how the use of a statistical threshold can be feasible to detect peculiar morphologies on specific topographic parameters (see Tarolli (2014) for a full review). In this case, the standard deviation threshold should be considered simply as an indicative measure to label most of the fibres related to the terraces within the open-pits (Fig. 9).

Fig. 10 shows radar graphs displaying the orientation of the correlation length, with respect to North, for the two mines, considering the whole maps (Fig. 9a and b), and the orientation only of those fibres having a SLLAC higher than one standard deviation of the SLLAC map (Fig. 9c and d).

If we consider the orientation of the complete SLLAC maps (Fig. 10a and b), it appears that the two study sites do not present noticeable differences. Mine I (Fig. 10a) seems to have a more prominent orientation in the direction of North–South. Mine II, on the other hand, seems to have a more random orientation (Fig. 10b), with a similar amount of fibres leaning in all cardinal directions. However, by focusing only on the orientation of those fibres that have a larger correlation length (SLLAC > σ_{SLLAC}, see Fig. 9c and d), the analysis of the orientation gives more useful insights. The terraces in mine I are clearly oriented in the North–South direction, with fewer areas leaning in the East–West direction (Fig. 10c). This could also be read as a measure of the shape of the mine: having more fibres leaning towards the North–South and fewer towards the East–West implies an open-pit with a rectangular shape with the longest side in the North–South direction. Instead, mine II presents fibres oriented in all cardinal directions, implying a more round (or square) shape in the mine area, having sides with similar lengths but opposite orientations.

5. Future challenges

Mining regions undergo abrupt and extensive land use changes, the impacts of which pose management challenges for mining companies and regulatory agencies (Sonter et al., 2014). Accurate quantification of the extent of mining activities is important for assessing how this land use can affect the landscape (Townsend et al., 2008); the utility of interfacing remote sensing and geographic information systems for effective environmental management of mining areas has already been emphasised (Rathore and Wright, 1993). However, most mine studies are generally qualitative, and they are based mostly on the detection of the changes in vegetation cover, rather than on the estimation of the mine's extent (see Townsend et al., 2008). This work provides a basis on which to automatically map the extent of mines at a given time, which could be used as a starting point for future research. For example, given the availability of multi-temporal surveys, it would be possible to track the changes in the extent of the mine. In addition, we could relate the extent of the mines to the amount of processes in the area (e.g. pollution, erosion, subsidence, etc.). As a final step, it could be possible to combine the two points and to analyse the effects of continued mining or mine reclamation on surface processes through time in mining landscapes. Modern surface mining techniques using heavy equipment can, in fact, produce dramatic ecological and hydrological alterations (Simmons et al., 2008). In addition, the orientation of the topographic surface or excavation face with respect to geologic features is of major significance in mine studies, given that the tectonic environment and history, or inheritance, of a given slope can determine if and how it fails (Rose and Scholz, 2009; Stead and Wolter, 2015). An adequate slope orientation determination is necessary to better integrate the work of the geomechanical group into the slope creation process (Grenon and Laflamme, 2011). Having a tool that automatically depicts the current main orientation of the terrace could offer new strategies to compare such information with available geological data in order to better understand the failure mechanisms when present; for example, to rule in or out the geological component. In addition, based on the orientation of the slope faces and using the geo-structural data derived from geomatic and engineering geological surveys, it could be possible to perform further analyses on slope stability (Francioni et al., 2015). Finally, by analysing the geomorphological features of terraces in different orientations, anthropogenic or natural activities that damaged the original terraces, such as landfilling, land-sliding and crumbling, could be easily identified. The integrity and stability of the terrace from the quantitative analysis of DSM, integrated

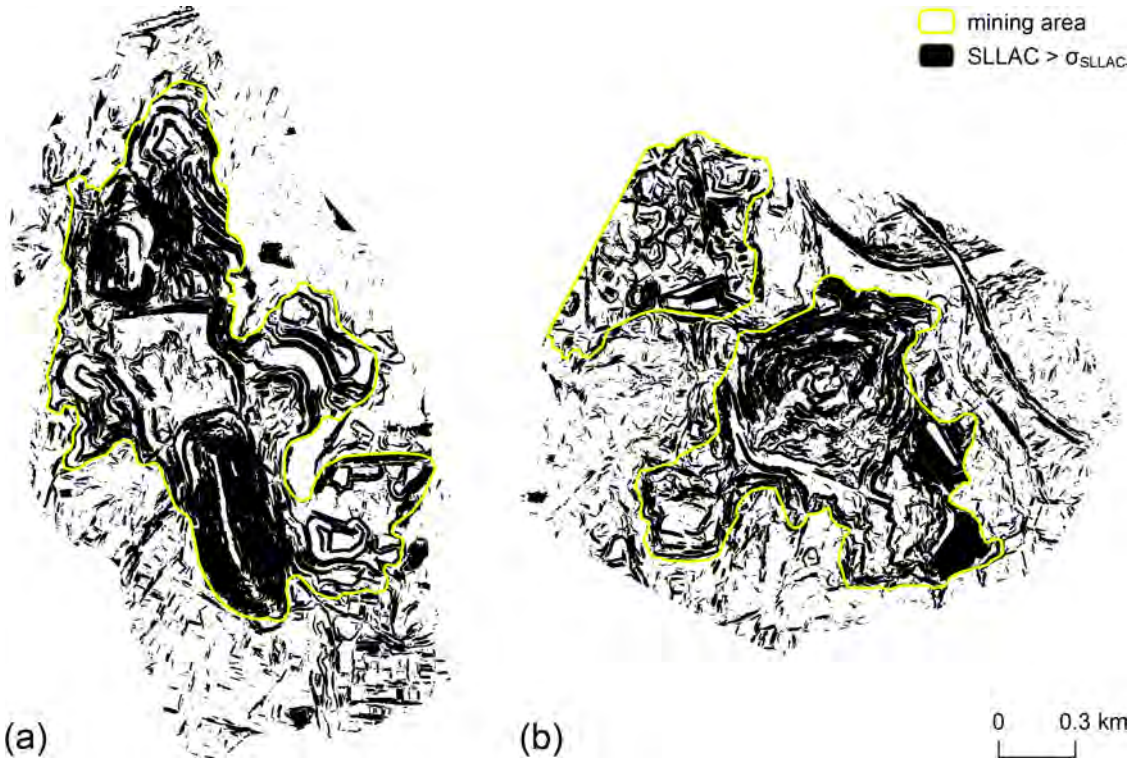

Fig. 9. Areas having correlation lengths larger than one standard deviation of SLLAC (a and b). The yellow boundaries represent the extraction areas where terraces are present.

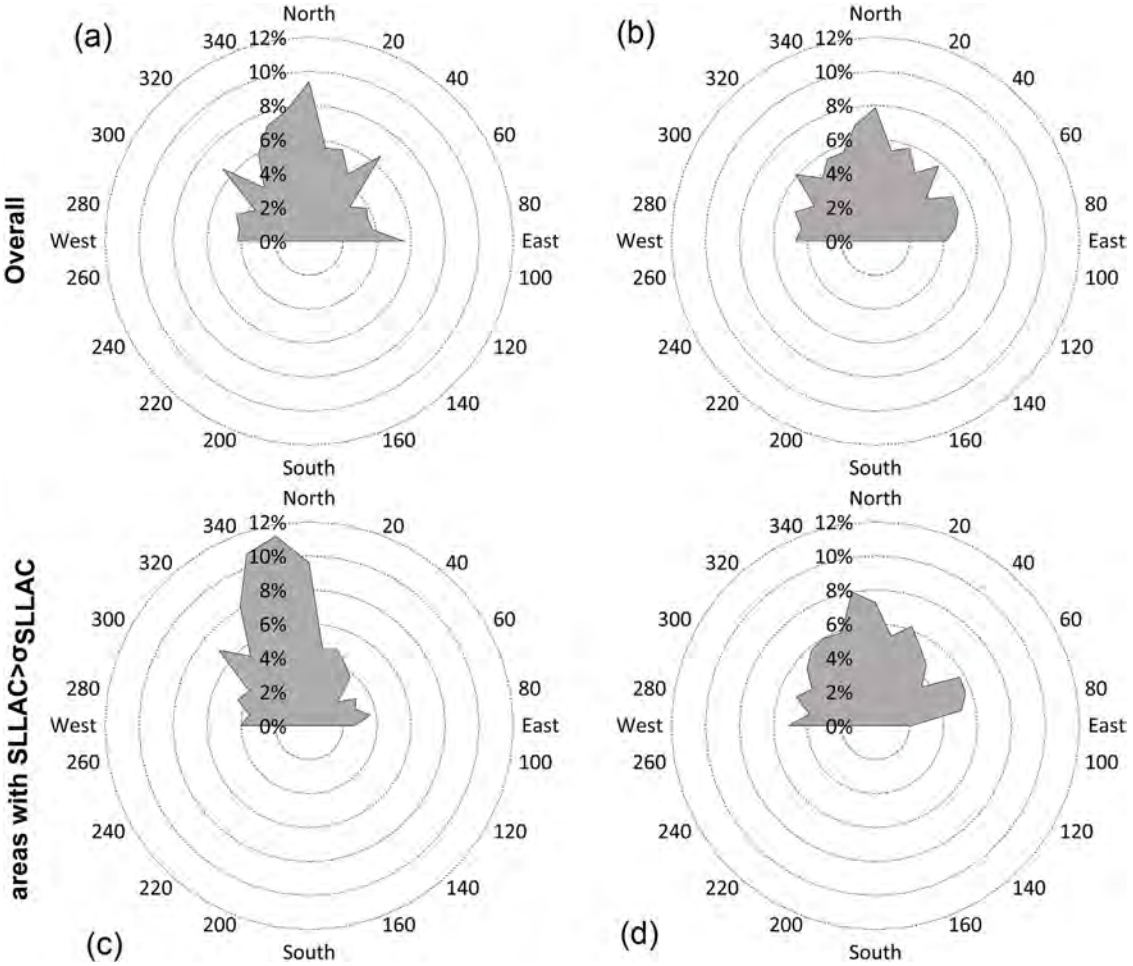

Fig. 10. Radar graphs of the orientation of the correlation lengths for the two mining sites, considering the overall SLLAC maps (a and b), and only those areas having a correlation length greater than one standard deviation of the SLLAC (c and d).

with available geological data and engineering data, can provide powerful support for decision-making regarding slope protection and mining plans.

6. Conclusions

A geomorphological characterisation of open-pit mining areas can provide a useful framework for a better understanding of mining environmental effects (e.g. erosion), but could also be useful when planning the most appropriate reclamation strategies. Along this line, this paper proposes a characterisation of the geomorphic features of open-pit mines using a rapid, low-cost methodology based on a novel landscape metric, SLLAC, and high-resolution topography derived by UAV and SfM. The results underline how the use of very high-resolution imagery taken with UAV and, afterwards, processed using the SfM technique, allows for the obtainment of a precise DSM in near real-time and at a very low cost. From this DSM, the analysis of the SLLAC and its derived parameters allows for the correct depiction of terraces, their orientation, and the extent of the open-pit. By analysing the Spc parameter and considering a polynomial approach that relates the increase in the *Spc* and the decrease in the terraced surface, we are able estimate the mine's extent in an automatic way, providing results comparable to the manual measurement from aerial photographs. Unfavourable combinations of directions of terraces compared to the directions of the geological structures can produce several local instabilities. A detection of the directions of the terraces, therefore, could provide useful information to be used in in geologic analyses for risk assessment. The proposed methodology offers a flexible tool to assess the mine's state rapidly and efficiently. Due to the UAV survey, the topographic information can be collected at any stage of the mine's life, and the proposed characterisation techniques could be used for large-scale topographic surveys and to detect potentially unstable conditions of slopes. Therefore, this could be a tool used to support sustainable environmental planning and to mitigate the consequences of anthropogenic alterations due to mining.

Acknowledgements

This research has been supported by China Geological Survey project "Mine environmental comprehensive investigation and evaluation" No. 1212011120029. The technical support for the UAV survey was provided by Sky View Technology Co., Ltd. (Taiwan). Data analysis resources were provided by the Interdepartmental Research Center of Geomatics (CIRGEO), at the University of Padova (Italy). The authors thank the anonymous reviewers for their advices and suggestions.

References

Abo Akel, N., Filin, S., Doytsher, Y., 2007. Orthogonal polynomials supported by region growing segmentation for the extraction of terrain from LiDAR data. Photogramm. Eng. Remote Sens. 73 (11), 1253–1266.
Badri, A., Nadeau, S., Gbodossou, A., 2011. Integration of OHS into risk management in an open-pit mining project in Quebec (Canada). Minerals 1, 3–29.
Colomina, I., Molina, P., 2014. Unmanned aerial systems for photogrammetry and remote sensing: A review. ISPRS J. Photogramm. Remote Sens. 92, 79–97.
Ellis, E.C., 2004. Long-term ecological changes in the densely populated rural landscapes of China. In: DeFries, R.S., Asner, G.P., Houghton, R.A. (Eds.), Ecosystems and Land Use Change. American Geophysical Union, Washington, DC, pp. 303–320.
Ellis, E.C., Wang, H., Xiao, H., Peng, K., Liu, X.P., Li, S.C., Ouyang, H., Cheng, X., Yang, L.Z., 2006. Measuring long-term ecological changes in densely populated landscapes using current and historical high resolution imagery. Remote Sens. Environ. 100, 457–473.
Ellis, E.C., 2011. Anthropogenic transformation of the terrestrial biosphere. Philos. Trans. R. Soc. A 369, 1010–1035.
Esterhuizen, G.S., Gürtunca, R.G., 2006. Coal mine safety achievements in the USA and the contribution of NIOSH research. J. S. Afr. Inst. Min. Metall. 106, 813–820.
Evans, I.S., 1980. An integrated system of terrain analysis and slope mapping. Zeitschrift fur Geomorphologie. Suppl. Bd. 36, 274–295.
Foley, J.A., DeFries, R., Asner, G.P., Barford, C., Bonan, G., Carpenter, S.R., 2005. Global consequences of land use. Science 309, 570–574.
Fonstad, M.A., Dietrich, J.T., Courville, B.C., Jensen, J.L., Carbonneau, P.E., 2013. Topographic structure from morion: a new development in photogrammetric measurement. Earth Surf. Processes Landforms 38, 421–430.
Foster, P.J., Parand, A., Bennett, J.G., 2008. Improving the safety performance of the UK quarrying industry through a behavioural based safety intervention. J. S. Afr. Inst. Min. Metall. 108, 683–690.
Francioni, M., Salvini, R., Stead, D., Giovannini, R., Riccucci, S., Vanneschi, C., Gullì, D., 2015. An integrated remote sensing-GIS approach for the analysis of an open pit in the Carrara marble district: Italy: slope stability assessment through kinematic and numerical methods. Comput. Geotech. 67, 46–63.
Grenon, M., Laflamme, A., 2011. Slope orientation assessment for open-pit mines, using GIS-based algorithms. Comput. Geosci. 37 (9), 1413–1424.
Hancock, G.R., Lowry, J.B.C., Moliere, D.R., Evans, K.G., 2008. An evaluation of an enhanced soil erosion and landscape evolution model: a case study assessment of the former Nabarlek uranium mine Northern Territory, Australia. Earth Surf. Process. Landforms 33, 2045–2063.
Haralick, R.M., Shapiro, L.G., 1992. Computer and Robot Vision, II. Addison-Wesley, pp. 316–317.
Hermanus, M.A., 2007. Occupational health and safety in mining – status, new developments, and concern. J. S. Afr. Inst. Min. Metall. 107, 531–538.
Herrera, G., Tomás, R., Vicente, F., Lopez-Sanchez, J.M., Mallorquí, J.J., Mulas, J., 2010. Mapping ground movements in open pit mining areas using differential SAR interferometry. Int. J. Rock Mech. Min. Sci. 47 (7), 1114–1125.
Heuvelink, G., Burrough, P., Stein, A., 1989. Propagation of errors in spatial modeling with GIS. Int. J. Geog. Inf. Syst. 3 (4), 303–322.
Hugenholtz, C.H., Whitehead, K., Brown, O.W., Barchyn, T.E., Moorman, B.J., LeClair, A., Riddell, K., Hamilton, T., 2013. Geomorphological mapping with a small unmanned aircraft system (sUAS): feature detection and accuracy assessment of a photogrammetrically-derived digital terrain model. Geomorphology 194, 16–24.
ISO 25178-2, 2013. Geometrical product specifications (GPS) – Surface texture: Areal – Part 2: Terms, definitions and surface texture parameters.
Jaakkola, A., Hyyppä, J., Kukko, A., Yu, X., Kaartinen, H., Lehtomäki, M., Lin, Y., 2010. A low-cost multi-sensoral mobile mapping system and its feasibility for tree measurements. ISPRS J. Photogramm. Remote Sens. 65, 514–522.
James, M.R., Robson, S., 2014. Mitigating systematic error in topographic models derived from UAVand ground-based image networks. Earth Surf. Processes Landforms 39, 1413–1420.
Javernick, L., Brasington, B., Caruso, B., 2014. Modeling the topography of shallow braided rivers using structure-from-motion photogramnmetry. Geomorphology 213, 166–182.
Lanter, D., Veregin, H., 1992. A research based paradigm for propagating error in layer-based GIS. Photogramm. Eng. Remote Sens. 58 (6), 825–833.
Lewis, J.P., 1995. Fast template matching. Vision Interface, 120–123.
Lin, C.W., Tseng, C.-M., Tseng, Y.-H., Fei, L.-Y., Hsieh, Y.-C., Tarolli, P., 2013. Recognition of large scale deep-seated landslides in forest areas of Taiwan using high resolution topography. J. Asian Earth Sci. 62, 389–400.
Lucieer, A., Turner, D., Diana, H.K., Robinson, S.A., 2014. Using an unmanned aerial vehicle (UAV) to capturemicro-topography of Antarctic moss beds. Int. J. Appl. Earth Obs. Geoinf. 27, 53–62.
Mesas-Carrascosa, F.J., 2014. Validation of measurements of land plot area using UAV imagery. Int. J. Appl. Earth Obs. Geoinf. 33, 270–279.
Mancini, F., Dubbini, M., Gattelli, M., Stecchi, F., Fabbri, S., Gabbianelli, G., 2013. Using unmanned aerial vehicles (UAV) for high-resolution reconstruction of topography: the structure from motion approach on coastal environments. Remote Sens. 5, 6880–6898.
Martín-Duque, J.F., Sanz, M.A., Bodoque, J.M., Lucía, A., Martín-Moreno, C., 2010. Restoring earth surface processes through landform design: a 13-year monitoring of a geomorphic reclamation model for quarries on slopes. Earth Surf. Processes Landforms 35, 531–548.
Micheletti, N., Chandler, J.H., Lane, S.N., 2014. Investigating the geomorphological potential of freely available and accessible structure-from-motion photogrammetry using a smartphone. Earth Surf. Processes Landforms, http://dx.doi.org/10.1002/esp.3648
Mossa, J., James, L.A., 2013. Impacts of mining on geomorphic systems. In: John Shroder, F. (Ed.), Treatise on Geomorphology. Academic Press, San Diego, pp. 74–95.
Nicolau, J.M., Asensio, E., 2000. Rainfall erosion of opencast coal-mine lands: ecological perspective. In: Haigh, M.J. (Ed.), Reclaimed Land: Erosion Control, Soils and Ecology. Balkema, Rotterdam, pp. 51–73.
d'Oleire-Oltmanns, S., Marzolff, I., Peter, K.D., Ries, J.B., 2012. Unmanned aerial vehicle (UAV) for monitoring soil erosion in Morocco. Remote Sens. 4, 3390–3416.
Osterkamp, W.R., Joseph, W.L., 2000. Climatic and hydrologic factors associated with reclamation. In: Barnishe, I.R., Darmody, R., Daniels, W. (Eds.), Reclamation of Drastically Disturbed Lands. American Society of Agronomy, Madison, pp. 193–216.
Openshaw, S., Charlton, M., Carver, S., 1991. Error propagation: a Monte Carlo simulation. In: Masser, I., Blackemore, M. (Eds.), Handling Geographic

Information: Methodology and Potential Applications. Longman Scientific and Technical, UK, pp. 78–102.
Passalacqua, P., Hillier, J.H., Tarolli, P., 2014. Innovative analysis and use of high resolution DTMs for understanding earth-surface processes. Earth Surf. Processes Landforms 39, 1400–1403.
Pirotti, F., Tarolli, P., 2010. Suitability of LiDAR point density and derived landform curvature maps for channel network extraction. Hydrol. Processes 24, 118–1197.
Pirotti, F., Grigolato, S., Lingua, E., Sitzia, T., Tarolli, P., 2012. Laser scanner applications in forest and environmental sciences. Ital. J. Remote Sens. 44 (1), 109–123.
Prosdocimi, M., Sofia, G., Dalla Fontana, G., Tarolli, P., 2015. Bank erosion in agricultural drainage networks: new challenges from Structure-from-Motion photogrammetry for post-event analysis. Earth Surf. Processes Landforms, http://dx.doi.org/10.1002/esp.3767
Ralston, A., Rabinowitz, P., 1978. A First Course in Numerical Analysis, Second edition. McGraw-Hill, New York, pp. 4.4–4.8.
Rathore, C.S., Wright, R., 1993. Monitoring environmental impacts of surface coal-mining. Int. J. Remote Sens. 14, 1021–1042.
Rigina, O., 2002. Environmental impact assessment of the mining and concentration activities in the Kola Peninsula, Russia, by Multidate remote sensing. Environ. Monit. Assess. 75 (1), 13–33.
Roering, J.J., Mackey, B.H., Marshall, J.A., Sweeney, K.E., Deligne, N.I., Booth, A.M., Handwerger, A.L., Cerovski-Darriau, C., 2013. 'You are HERE': connecting the dots with airborne lidar for geomorphic fieldwork. Geomorphology 200, 172–183.
Rose N., Scholz M., 2009. Analysis of complex deformation behaviour in large open pit mine slopes using the Universal Distinct Element Code (UDEC) In Proceedings: Slope Stability 2009, International Symposium on Rock Slope Stability in Open Pit Mining and Civil Engineering Santiago.
Schertzer, D., Tchiguirinskaia, I., Lovejoy, S., 2013. Multifractality: at least three moments! in interactive comment on Just two moments! A cautionary note against use of high-order moments in multifractal models in hydrology by F. Lombardo et al. Hydrol. Earth Syst. Sci. Discuss. 10, C3103–C3109 www.hydrol-earth-syst-sci-discuss.net/10/C3103/2013/.
Schertzer, D., Lovejoy, S., 1989. Nonlinear variability in geophysics: multifractal analysis and simulation. In: Pietronero, L. (Ed.), Fractals: Physical Origin and Consequences. Plenum, New-York, pp. 49–79.
Severin, J., Eberhardt, E., Leoni, L., Fortin, S., 2014. Development and application of a pseudo-3D pit slope displacement map derived from ground-based radar. Eng. Geol. 181, 202–211.
Sibson, R., 1981. A brief description of natural neighbor interpolation. In: Barnett, V. (Ed.), Interpreting Multivariate Data. Wiley, Chichester, pp. 21–36.
Simmons, J.A., Currie, W.S., Eshleman, K.N., Kuers, K., Monteleone, S., Negley, T.L., 2008. Forest to reclaimed mine land use change leads to altered ecosystem structure and function. Ecol. Appl. 18, 104–118.
Slatton, K.C., Carter, W.E., Shrestha, R.L., Dietrich, W.E., 2007. Airborne laser swath mapping: achieving the resolution and accuracy required for geosurficial research. Geophys. Res. Lett. 34, L23S10, http://dx.doi.org/10.1029/2007GL031939
Sofia, G., Pirotti, F., Tarolli, P., 2013. Variations in multiscale curvature distribution and signatures of LiDAR DTM errors. Earth Surf. Processes Land 38, 1116–1134.
Sofia, G., Mariniello, F., Tarolli, P., 2014. A new landscape metric for the identification of terraced sites: the slope local length of auto-correlation (SLLAC). ISPRS J. Photogramm. Remote Sens. 96, 123–133.
Sonter, L.J., Moran, C.J., Barrett, D.J., Soares-Filho, B.S., 2014. Processes of land use change in mining regions. J. Cleaner Prod. 84, 494–501.
Stead, D., Wolter, A., 2015. A critical review of rock slope failure mechanisms: the importance of structural geology. J. Struct. Geol. 74, 1–23.
Stout, K.J., Sullivan, P.J., Dong, W.P., Mainsah, E., Luo, N., Mathia, T., Zahouani, H., 1994. The development of methods for the characterization of roughness on three dimensions. Publication no. EUR 15178 EN of the Commission of the European Communities. Luxembourg.
Tarolli, P., 2014. High-resolution topography for understanding earth surface processes: opportunities and challenges. Geomorphology 216, 295–312.
Tarolli, P., Arrowsmith, J.R., Vivoni, E.R., 2009. Understanding earth surface processes from remotely sensed digital terrain models. Geomorphology 113, 1–3.
Tarolli, P., Preti, F., Romano, N., 2014. Terraced landscapes: From an old best practice to a potential hazard for soil degradation due to land abandonment. Anthropocene 6, 10–25.
Tarolli, P., Sofia, G., Calligaro, S., Prosdocimi, M., Preti, F., Dalla Fontana, G., 2015. Vineyards in terraced landscapes: new opportunities from lidar data. Land Degrad. Dev. 26, 92–102.
Toy, T.J., Hadley, R.F., 1987. Geomorphology of Disturbed Lands. Academic Press, London.
Townsend, P.A., Helmers, D.P., Kingdon, C.C., McNeil, B.E., de Beurs, K.M., Eshleman, K.N., 2008. Changes in the extent of surface mining and reclamation in the Central Appalachians: 1976–2006. Remote Sens. Environ. 113, 62–72.
Tseng, C.-M., Lin, C.-W., Dalla Fontana, G., Tarolli, P., 2015. The topographic signature of a Major Typhoon. Earth Surf. Processes Landforms, http://dx.doi.org/10.1002/esp.3708
Watts, A.C., Ambrosia, V.G., Hinkley, E.A., 2012. Unmanned aircraft systems in remote sensing and scientific research: classification and considerations of use. Remote Sens. 4, 1671–1692.
Westoby, M.J., Brasington, J., Glasser, N.F., Hambrey, M.J., Reynolds, J.M., 2012. 'Structure-from-motion' photogrammetry: a low-cost, effective tool for geosciences applications. Geomorphology 17, 300–314.
Wilkinson, B.H., 2005. Humans as geologic agents: a deep-time perspective. Geology 33 (3), 161–164.
Wilkinson, B.H., McElroy, B.J., 2007. The impact of humans on continental erosion and sedimentation. Geol. Soc. Am. Bull. 119 (1/2), 140–156.
Woodget, A.S., Carbonneau, P.E., Visser, F., Maddock, I., 2015. Quantifying submerged fluvial topography using hyperspatial resolution UAS imagery and structure from motion photogrammetry. Earth Surf. Processes Landforms. 40, 47–64.
Vanacker, V., Bellin, N., Molina, A., Kubik, P.W., 2014. Erosion regulation as a function of human disturbances to vegetation cover: a conceptual model. Landscape Ecol. 29, 293–309.
Vidal, O., Goffè, B., Arndt, N., 2013. Metals for a low-carbon society. Nature 6, 894–896.
Zhangtao, Z., 2010. Analysis on occupational-related safety fatal accident reports of China, 2001–2008. Saf. Sci. 48, 640–642.